ACS Catalysis

pubs.acs.org/acscatalysis Research Article

Identity, Evolution, and Acidity of Partially Framework-Coordinated Al Species in Zeolites Probed by TMP ^{31}P-NMR and FTIR

Zhili Wang, Dong Xiao, Kuizhi Chen,* Caiyi Lou, Lixin Liang, Shutao Xu,* and Guangjin Hou*

Cite This: ACS Catal. 2023, 13, 4960−4970 Read Online

ACCESS | Metrics & More | Article Recommendations | Supporting Information

ABSTRACT: Increasing research has shown that active sites in zeolite catalysts are structurally and spatially complex, which poses challenges to effective characterization methods, especially for the high demand in pursuing molecular-level understanding of the nature of the active sites. Herein, using trimethylphosphine (TMP) as a probe molecule, the species giving rise to ^{31}P NMR resonance at −58 ppm, which is typically recognized as TMP physically adsorbed on unreactive species, is found to possess more catalytic meanings as the TMP bindings are proven to be strong. NMR-assisted ^{31}P-^{27}Al internuclear distance measurement and a comprehensive set of two-dimensional (2D) heteronuclear correlation (HETCOR) (^{1}H-^{31}P, ^{31}P-^{27}Al, and ^{27}Al-^{1}H) NMR experiments explicitly demonstrate that the TMP-binding site is neither a bridging acid site (BAS) nor a Lewis acid site (LAS), but special Al−OH groups, i.e., Al−OH···P$(CH_3)_3$. Further evidence including postsynthetic treatments and ^{31}P-^{31}P homonuclear NMR correlation experiments exclusively shows that these Al−OH groups originate from the partially bonded framework Al(IV)-2 species recently reported. By linking IR and ^{1}H NMR spectroscopy, new insights of Al(IV)-2 (essentially Brønsted sites) and framework-bonded Lewis sites are provided. Finally, ^{31}P-^{31}P homonuclear correlation experiment was capable of ruling out chemical exchange from spin diffusion and thereby exclusively demonstrates that the "BAS and Al(IV)-2" is in shorter spatial distance than that of "BAS and LAS".

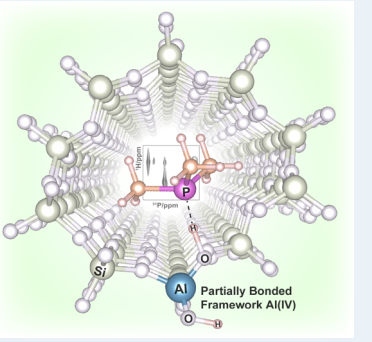

KEYWORDS: *zeolite, acid site, ^{31}P NMR, TMP probe molecule, FTIR, site proximity*

INTRODUCTION

Zeolite catalysts have been playing crucial roles in modern industrial processes owing to their well-defined microscopic pore topology and intrinsic acid sites[1,2] but with uncertainties remaining in the active site structures and their true catalytic functions. Bridging acid site (BAS) is usually considered as the primary active site which originates from the charge compensating proton on the tetrahedral framework aluminum site,[3−5] and Lewis acid site (LAS) associated with extra-framework aluminum (EFAl) species is another important type of active site, usually believed to form upon hydrothermal treatments, i.e., steaming or calcination processes.[6−9] Recently, a second BAS has been revealed by ultra-high-field NMR, showing that partially bonded framework aluminum species could widely retain a tetrahedral coordination, i.e., $(SiO)_{4-n}$−$Al(OH)_n$, or Al(IV)-2 for simplicity, and consequently produce a charge balanced acidic proton and Al−OH groups that could also be acidic.[10−12] The Al(IV)-2 species can as well be created upon thermal treatments similar to that for EFAls, making its differentiation from EFAls challenging. Nonetheless, it is believed that both LAS and Al(IV)-2 play unique and important roles in zeolites' catalytic performances, via intrinsic or synergistic effects,[13−15] rendering their elaborate structural elucidations urgent.

Solid-state NMR has emerged as one of the most powerful techniques to pursue atomic-scale structure of zeolites, via direct or indirect methods.[16−18] The direct approach refers to NMR detection of intrinsic atoms in the catalyst itself, via, i.e., ^{1}H, ^{27}Al, ^{29}Si, or ^{17}O,[13,19,20] while the indirect approach, in comparison, exploits the information on selected probe molecules interacting with active sites or interested species.[21,22] Trimethylphosphine (TMP) is an effective probe molecule for characterizing solid acid properties, owing to the large chemical shift range, high sensitivity, the relatively simple spin-1/2 nature of the ^{31}P NMR,[23,24] as well as its capability of characterizing acidic strengths of Brønsted and/or Lewis acid sites.[25,26] More importantly, the ^{31}P-TMP NMR approach is capable of providing detailed features about proximity, concentration, and distribution of acid sites.[21] BAS and LAS in zeolites have been widely investigated and documented by adopting the ^{31}P-TMP NMR approach,[26−28] whereas controversy signals/species remain. Unless otherwise noted, "BAS" is specifically referred to the "bridging acid site" in this manuscript to avoid potential confusions.

Received: February 14, 2023
Revised: March 15, 2023
Published: March 28, 2023

In this contribution, with a comprehensive NMR exploration of TMP-probed MFI zeolites, it is revealed that a TMP-bound species appearing at ^{31}P chemical shift of ca. −58 ppm, usually treated as unimportant physisorbed TMP molecules,[29,30] is indeed TMP bound to important catalytic sites. As a reference, Yi et al. generically assigned the signals at −56 ∼ −60 ppm to TMP adsorbed on weakly acidic Si−OH groups;[25] Kao and Grey tended to suggest that the −58 ppm resonance was caused by a very weakly bound or physisorbed TMP molecule,[31] while other studies suggested that it accounts for Lewis-bound TMP adducts.[32,33] Here, assisted by a combined set of modern ssNMR techniques, including one-dimensional (1D) ^{31}P MAS and ^{31}P{^{27}Al} rotational-echo adiabatic-passage double-resonance (REAPDOR),[34,35] and two-dimensional (2D) ^{1}H-^{31}P heteronuclear correlation (HETCOR),[36,37] ^{31}P-^{27}Al dipolar-based heteronuclear multiple-quantum coherence (*D*-HMQC),[38,39] ^{27}Al-^{1}H dipolar-based refocused insensitive nuclei enhanced by polarization transfer (*D*-RINEPT) using the recently reported windowed phase-modulated rotary resonance (PMRR) recoupling method,[40−42] ^{31}P-^{31}P combined *R*2*v* *n*-driven (CORD)/radio-frequency dipolar recoupling (RFDR),[43−46] and ^{27}Al multiple-quantum magic-angle spinning (MQMAS) experiments,[47,48] we were able to show evidently that the $\delta(^{31}P)$ = −58 ppm resonance exclusively arise from TMP molecules adsorbed on Al−OH groups, i.e., Al−OH···P$(CH_3)_3$, and such Al species is tetrahedrally coordinated and possesses a much smaller quadrupolar coupling constants C_Q compared with that of TMP-adsorbed LAS, and therefore excludes the possibility of being Lewis-type adsorptions. Also, considering that TMP-adsorbed BAS sites give rise to ^{31}P signal at −5 ppm, the only possible explanation is that the −58 ppm signal arises from the recently reported partially framework-coordinated Al(IV) species or Al(IV)-2 as usually denoted.[10,11,13] By linking IR and ^{1}H NMR spectroscopical results, new insights of Al(IV)-2 (essentially Brønsted sites) and framework-bonded Lewis sites are provided. Furthermore, 2D ^{31}P-^{31}P correlation NMR experiments reveal closer proximity between the TMP-adsorbed BAS and Al(IV)-2 sites, compared to that between the BAS and LAS sites, providing critical information to clarify the arguments in the intriguing synergistic effects in zeolite catalysts.[10,13,14,49−53] The comprehensive elucidation of the TMP-Al(IV)-2 species could shed light on unraveling the complex BAS-LAS-silanol-aluminol network structure of zeolites in the future.

RESULTS AND DISCUSSION

The primary ZSM-5 zeolite catalyst used in this work is purchased from Nankai University Catalyst Co., Ltd., China, with Si/Al = 19. The parent and calcined (at 750 °C) HZSM-5 zeolites were denoted as P-ZSM-5 and C-ZSM-5, respectively. Unless otherwise noted, all catalysts are presented in their proton forms. Calcination and dehydration treatment details are described in the Supporting Information. As demonstrated by XRD in Figure S1, the structural integrity of ZSM-5 zeolite remains virtually intact after the calcination treatment.

Apart from the more commonly implemented ^{1}H and ^{27}Al NMR characterization as direct detection approaches, TMP-^{31}P NMR is well known for its unique advantages in resolving and quantifying the binding sites such as BAS, LAS, and hydroxyl groups. A group of characteristic ^{31}P signals is observed in TMP-treated HZSM-5, i.e., 26, 15, −5, −48, and −62 ppm,[21] as shown in the single-pulse and ^{31}P{^{1}H} cross-polarization (CP) MAS NMR spectra on the C-ZSM-5 catalyst in Figure 1, and same resonances are observed in P-ZSM-5

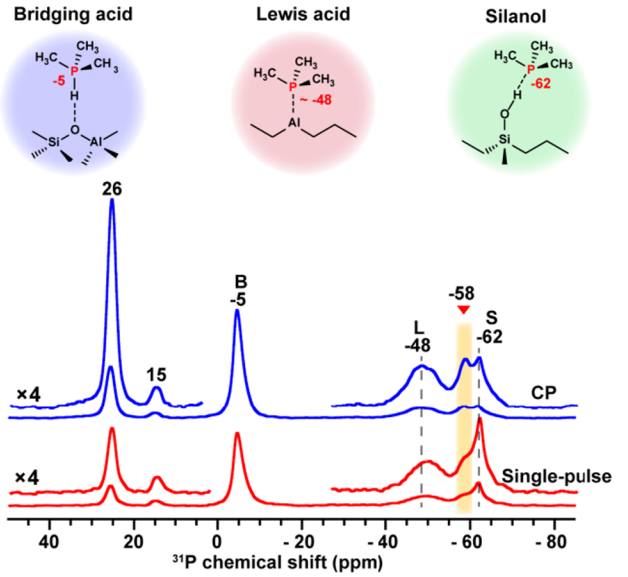

Figure 1. ^{31}P{^{1}H} CP (blue) and single-pulse ^{31}P MAS NMR (red) spectra of TMP adsorbed on dehydrated C-ZSM-5. TMP adsorbed on Brønsted acid site, Lewis acid site, and silanols is denoted as "B", "L", and "S" in the spectrum and with their structures illustrated in the top schemes. The highlighted −58 ppm species remain structurally elusive.

catalyst but with variation of the peak intensities, especially the more intense peak at −5 ppm and weaker peaks at −48 and −58 ppm, as shown in the P-ZSM-5 vs C-ZSM-5 comparison in Figure S2a. Usually, the 26, −5, −48, and −62 ppm signals are less debated, typically assigned to $P(CH_3)_4^+$ generated by the disproportionation reaction that consumes a BAS,[54] $TMPH^+$ formed by TMP adsorbed on BAS (denoted "B"),[55,56] TMP bound to LASs (denoted "L"),[30,57,58] and TMP physically adsorbed on Si−OH groups (denoted "S"), respectively.[27,30] The 15 ppm signal is presumably related to Fe impurities or silanols (vide infra, ^{31}P-^{31}P CORD) in the catalyst and shall not be critical to the structural interpretation.[56,59,60] The −58 ppm signal as highlighted in the shaded area in Figure 1, however, has remained controversial and is usually treated as physisorbed TMP signals similar to those at −62 ppm.[24,25,29,30] However, the spectrum clearly shows that the −58 and −62 ppm signals are different as the latter is significantly diminished in the CP spectrum, and the much lower intensity of the −62 ppm signal is likely caused by high mobility of TMP molecules due to the weak physical adsorption. Therefore, such a difference indicates that the −58 ppm TMP may not be weakly bound species. ^{27}Al and ^{1}H NMR spectra were also obtained, as illustrated in Figure S3, but provide no critical information to the identity of the −58 ppm species. However, thanks to the high NMR sensitivity of ^{27}Al, ^{1}H, and ^{31}P due to their high natural abundance and/or large gyromagnetic ratios, fine and invaluable structural details can be investigated by employing a series of NMR experiments to probe internuclear spatial correlation or bond connectivity of ^{1}H-^{31}P, ^{1}H-^{27}Al, ^{31}P-^{27}Al, and ^{31}P-^{31}P, which will be presented elaborately in the following discussion.

https://doi.org/10.1021/acscatal.3c00714
ACS Catal. 2023, 13, 4960−4970

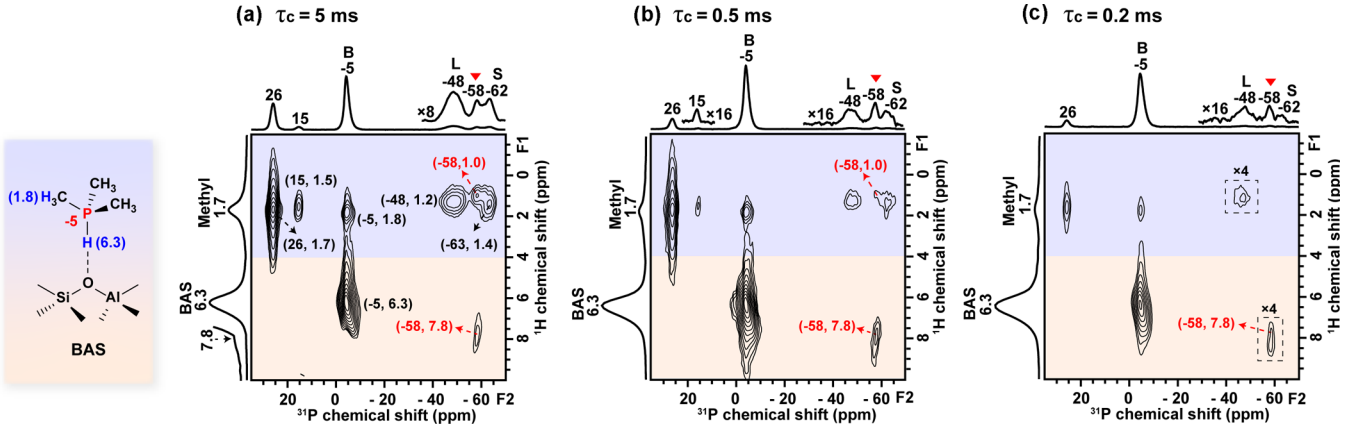

Figure 2. 2D ^{1}H-^{31}P HETCOR MAS NMR spectra (with ^{31}P *J*-decoupling) of TMP adsorbed on dehydrated C-ZSM-5 recorded with a contact time of (a) 5 ms, (b) 0.5 ms, and (c) 0.2 ms. All spectra are acquired at 14.1 T. Signals in the upper region of all spectra arise from the methyl groups on TMP molecules, and signals in the lower region arise from acid protons associated to the catalyst, as denoted in the structural scheme on the left, with TMP-BAS as an example.

Identity of the −58 ppm Species. 2D ^{1}H-^{31}P HETCOR MAS NMR spectra (with ^{31}P *J*-decoupling) were acquired to reveal the proximity information between the H and P atoms, as shown in Figure 2, where the TMP-treated C-ZSM-5 catalyst was chosen as it provides relatively higher intensity of the −58 ppm signal. Three contact times of τ_c = 5, 0.5, and 0.2 ms were applied to differentiate the dipolar coupling-dependent correlations as it reflects spatial distance and/or molecular mobilities. In general, along the F_1 dimension, the proton signals are identified in two regions, at ca. 1.7 and 6.3 ppm, which correspond to TMP-methyl groups and the zeolite's BAS protons adsorbed with TMP molecule (see the schematic structure), respectively, as indicated in the F_1 projections. The relative intensity between the methyl and BAS proton signals is very different in the HETCOR and 1D ^{1}H MAS NMR spectra, as comparing the F_1 projections in Figures 2 and S3b. The much-diminished methyl signal in the HETCOR spectrum is resulted from the much weaker H···P dipolar coupling interaction, caused by longer H···P distance and rapid motional averages of the methyl group.[25,37] The spectrum recorded with the long contact time of 5 ms maps a full set of cross-peaks with both strong and weak dipolar couplings. Briefly, along the F_1 dimension, the signals in the $\delta(^{1}H)$ < 4 ppm region, i.e., correlation peaks at (−5, 1.8), (−48, 1.2), (−62, 1.0), and (−58, 1.0), arise from TMP-methyl groups, and the signals in the $\delta(^{1}H)$ > 4 region, i.e., (−5, 6.3) and (−58, 7.8), arise from protons originally associated to zeolite itself. Notably, all ^{31}P species (as introduced in Figure 1) are correlated with methyl protons as it is an intrinsic group in the TMP molecule. The presence and absence of cross-peaks in the $\delta(^{1}H)$ > 4 region provide crucial information for structural elucidations. Signals at $\delta(^{31}P)$ = 26 and 15 ppm are not critical and thus are not discussed in detail. Reasonably, BAS generates a signal in this region but LAS does not, because the former yields Al−OH···P(CH_3) and the latter yields Al−P(CH_3), which offers an efficient way to distinguish between bridging (or Brønsted) and Lewis acid sites. The physisorbed TMP species at $\delta(^{31}P)$ = −62 only yields a correlation signal at the methyl region, which is also reasonable as usually very weak dipolar coupling is created upon physisorption. What is intriguing is that the $\delta(^{31}P)$ = −58 species yields a second cross-peak at the $\delta(^{1}H)$ > 4 ppm region, indicating that TMPs are adsorbed on a bridging or Brønsted type of acid site. By reducing the contact time to 0.5 and 0.2 ms, signals with weak dipolar couplings disappear or get significantly attenuated, but the (−58, 7.8) signal remains visible, suggesting short H···P distance and immobility of the H/P pair. It should be noted that the (−58, 1.0) signal disappears at τ_c = 0.2 ms despite it being intramolecular correlation. In all, the experimental results explicitly show that the $\delta(^{31}P)$ = −58 ppm signal is resulted from TMP strongly adsorbed on −OH groups, which should be an Al−OH rather than Si−OH, as the latter is known to be nonacidic.

^{31}P{^{27}Al} CP REAPDOR MAS NMR was subsequently carried out to measure the ^{31}P-^{27}Al heteronuclear dipolar interaction and their distance information.[34,35] Typically, a difference spectrum (ΔS) is obtained by subtracting a REAPDOR dephased spectrum (S') from the nondephased reference spectrum (S_0) to reveal the existence of the dipolar coupling interactions, as demonstrated in Figure 3a, where $\delta(^{31}P)$ = 26, −5, −48, and the −58 ppm species show positive peaks in the ΔS spectrum, indicating proximate P···Al distances in all these species. As a comparison, such dephasing is not observed on the TMP-physisorbed −62 ppm peak, which is believed to arise from TMP adsorbed on Si−OH groups. In addition, the signal at −58 ppm has less dipolar dephasing compared with the resonance at −48 ppm (TMP molecules adsorbed on LAS), indicating weaker dipolar interaction or longer spatial proximity between ^{31}P and ^{27}Al spins for the former. Quantitative internuclear distances can be obtained by evaluating the dephasing curve, i.e., by plotting $\Delta S/S_0$ vs recoupling time, and the ^{31}P-^{27}Al dipolar coupling constants (DCC) can be extracted by fitting the curves to a well-known function as[34]

$$\frac{\Delta S}{S_0}(\lambda) = 0.63(1 - e^{-(3.0\lambda)^2}) + 0.2(1 - e^{-(0.7\lambda)^2}) \quad (1)$$

where the parameter $\lambda = \tau \times$ DCC. The RF field strength of ^{27}Al was 83 kHz, corresponding to the adiabaticity parameter $\alpha = \upsilon_1^2/(\upsilon_Q\upsilon_r)$, where υ_1 is the ^{27}Al RF frequency, υ_Q is the quadrupolar frequency, and υ_r is the MAS frequency, i.e., 8 kHz. Note that it usually requires α > 0.5 for reliable fitting results,[34] which can be easily satisfied at the current condition, i.e., υ_r = 8 kHz and υ_Q < 0.6 MHz (vide infra, ^{31}P-^{27}Al *D*-HMQC). The extracted ^{31}P-^{27}Al DCC is 193 Hz, which corresponds to a spatial distance of 4.04 Å as shown in Figure

https://doi.org/10.1021/acscatal.3c00714
ACS Catal. 2023, 13, 4960−4970

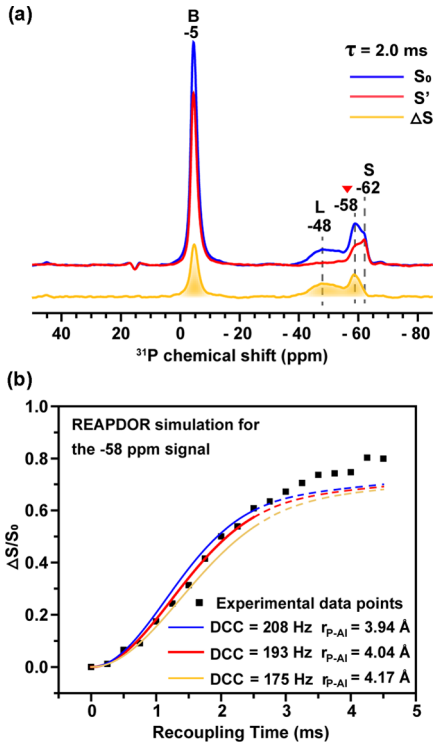

Figure 3. (a) $^{31}P\{^{27}Al\}$ CP REAPDOR spectra of TMP adsorbed on dehydrated C-ZSM-5 recorded with a recoupling time of 2.0 ms. (b) $^{31}P\{^{27}Al\}$ CP REAPDOR build-up curve of the $\delta(^{31}P)$ = −58 ppm signal of the sample from (a) with experimental data points and fitted curves indicated in the figure. All spectra are acquired at 9.4 T. Note that the long recoupling time region larger than ca. 2.5 ms (dashed lines) is not used for fitting due to the known complexity of long recoupling times.

3b. The long recoupling time region larger than ca. 2.5 ms (dashed lines) is not used for fitting as it may be perturbed by long-distance Al atoms. Similar fittings were also performed on LAS and BAS sites at −48 and −5 ppm as shown in Figure S4a,b. Here, in addition to calcined catalysts, steamed and AHFS-washed HZSM-5 catalysts were also investigated ("steaming" as another thermal treatment for dealumination but with the presence of water vapor and "AHFS-wash" as a postsynthetic method to remove EFAls and Al(IV)-2, vide infra). The ^{31}P-^{27}Al distance was determined to be ca. 2.45 Å for LAS in both calcined and steamed ZSM-5 catalysts (only the calcined sample, i.e., "C-ZSM-5," is illustrated in Figure S4a for simplicity), which is well in line with both experimental and theoretical results (2.3∼2.5 Å) in previous reports.[25,61] Such results can unambiguously exclude the possibility of the origin of the −58 ppm resonance being LAS and further confirm its assignment as TMP adsorbed on Al−OH groups. Although Al−OH can exist in totally dislodged EFAl and partially framework-coordinated aluminum sites, as discussed in several arguments,[12,53,62,63] the former can be ruled out as TMP would directly adsorb on the Al atom instead of Al−OH in that case.

The fitted ^{31}P-^{27}Al distance of the BAS signal at −5 ppm is ca. 4.8 Å, which however, is significantly longer than the distance reported in the literature, e.g., 3.95 Å by Grey and co-workers.[64] Such a discrepancy could be rationalized to motional/dynamic reasons as Grey's result was obtained using $^{27}Al\{^{31}P\}$ REDOR at −150 °C, given TMP-BAS binding is not as strong as that for TMP-LAS. It is well known that higher mobilities result in reduced DCC (or longer apparent distances). Also, intriguingly, it is found that the calcined and AHFS-washed catalyst result in similar dephasing curves, but the steamed catalyst yielded an apparently deviated curve with a larger apparent dipolar coupling interaction, as shown in Figure S4c, indicating more rigid local environments in the steamed sample (mostly likely due to hydrogen bonding environment). This result agrees well with the recent finding that dealumination favorably occurs at paired BAS sites.[13] Furthermore, the shorter distance 4.04 Å of Al(IV)-2 compared to 4.8 Å of the latter also suggests that Al(IV)-2 has a more complex environment, which can stabilize the adsorbed TMP molecules as its measured distance is close to Grey's result at a "frozen" condition, i.e., −150 °C and 3.95 Å. With all the REAPDOR results on the different postsynthetically treated catalysts, it is most reasonable to assign the −58 ppm signal as TMP molecules adsorbed on partially coordinated Al(IV)-2 species.

Structural Elucidation of the −58 ppm Species. ^{27}Al, being a quadrupolar spin, is sensitive to local electron environments, which is encoded in a set of quadrupolar parameters, i.e., isotropic chemical shift δ_{iso}, quadrupolar coupling constant C_Q, and the asymmetry parameter η_Q.[65,66] Two-dimensional ^{27}Al MQMAS NMR has been shown to efficiently separate Al species and address local bonding/coordination environments for zeolite catalysts,[67,68] and therefore, is employed here to further investigate the Al species after TMP treatment. As shown in the ^{27}Al MQMAS spectrum for TMP-treated C-ZSM-5 in Figure 4a, three main signals are clearly separated, denoted $Al_{IV,a}$, $Al_{IV,b}$, and Al_V, which are marked in blue, red, and green, respectively. The green signal centers at (33, 40) and can be assigned to penta-coordinated Al species (Al_V) due to its characteristic ^{27}Al chemical shift around the 30−40 ppm region.[69,70] The blue and red signals correspond to tetrahedrally coordinated Al species $Al_{IV,a}$ and $Al_{IV,b}$, possessing small and large C_Q values, respectively, indicated by the narrow and broad/horizontal patterns along the F_2 dimension as has been demonstrated clearly in the literature.[47,71] It should be noted that although the chemical shift of $Al_{IV,b}$ in the indirect dimension appears at ca. 70 ppm, its actual δ_{iso} is around 59 ppm (but clearly with chemical shift/quadrupolar shift distributions due to the broad spectral pattern[47]) as shown in a typical analysis of quadrupolar parameters in Figure S5, indicating that the aluminum in the TMP-Lewis acid adduct is tetrahedrally coordinated, which accounts for the assignment of this species as Al_{IV}. It is also worth mentioning that although the MQMAS spectrum appears similar to those of the hydrated proton-formed zeolites,[10,11] they shall not be compared directly as P atoms directly participate in the Al bonding configurations in this case.

To attain more in-depth structural information of the Al species, ^{31}P-^{27}Al and ^{27}Al-^{1}H 2D correlation spectra were acquired to provide internuclear spatial proximities. In detail, 2D ^{31}P-^{27}Al *D*-HMQC[38,39] and ^{27}Al-^{1}H *D*-RINEPT with wPMRR recoupling[40−42] experiments were carefully chosen to obtain the correlations with optimal sensitivities after inspecting the spin−lattice relaxation times (T_1) of ^{27}Al, ^{31}P, and ^{1}H, to best accommodate selections of short T_1 nuclei/excitation channel and high gyromagnetic ratio (γ) nuclei/detection channel configurations, and it should be noted that ^{31}P *J*-decoupling was applied during acquisition in the ^{27}Al-^{1}H *D*-RINEPT experiment. As shown in the ^{31}P-^{27}Al *D*-HMQC spectrum in Figure 4b, the first noticeable observation is the

https://doi.org/10.1021/acscatal.3c00714
ACS Catal. 2023, 13, 4960−4970

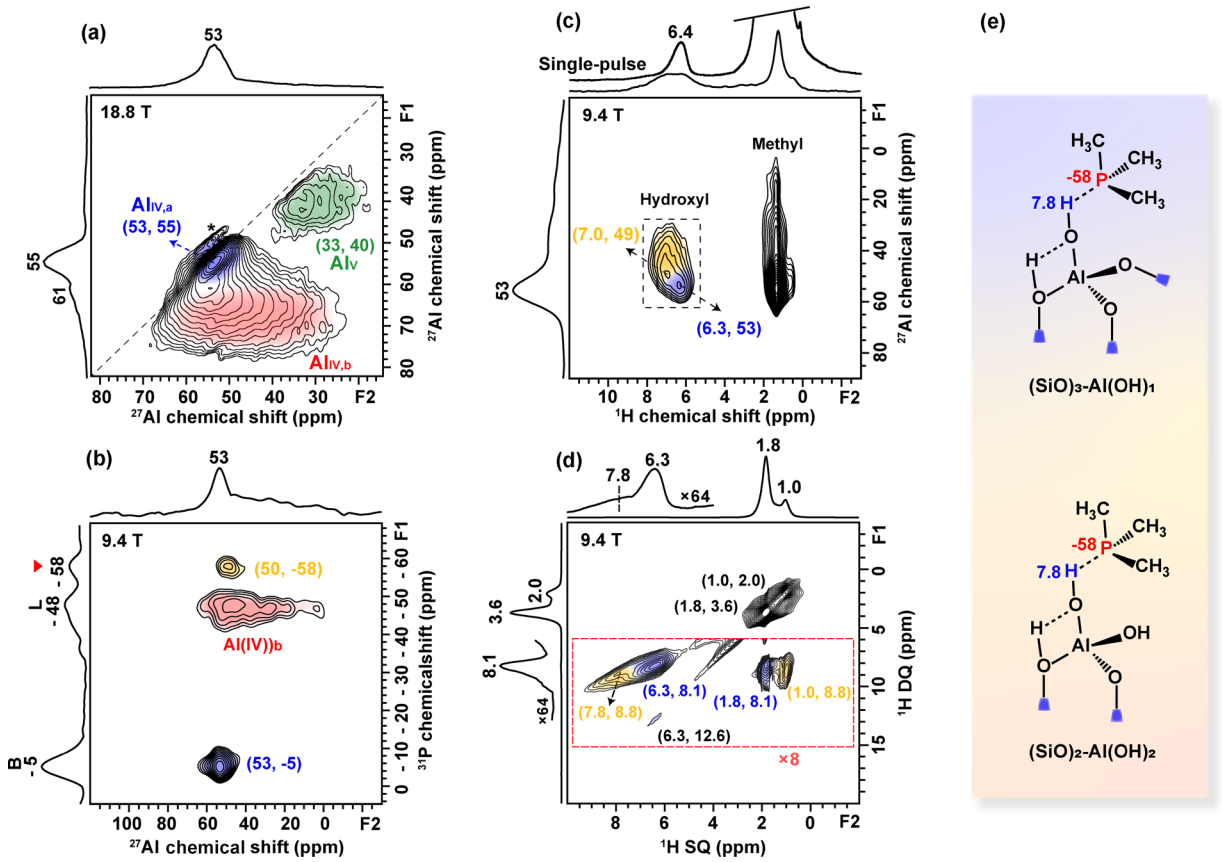

Figure 4. (a) ^{27}Al MQMAS, (b) ^{31}P-^{27}Al *D*-HMQC, (c) ^{27}Al-^{1}H *D*-RINEPT (^{31}P *J*-decoupling applied during ^{1}H acquisition), and (d) ^{1}H DQ-SQ MAS NMR spectra (with ^{31}P *J*-decoupling) of TMP adsorbed on dehydrated C-ZSM-5. (e) Schematic representations of TMP adsorbed on Al−OH group associated to partially framework-bonded species $(SiO)_{4-n}$−Al$(OH)_n$ with n = 1 and 2. Asterisks in (a) denote truncated signals of the $Al_{IV,a}$ species which possess relatively long T_2 values.

absence of Al_V species, indicating it may not be titrated by TMP molecules. $Al_{IV,b}$ is clearly related to the $\delta(^{31}P)$ = −48 ppm signal and thus can be unambiguously assigned to TMP-LAS. The $Al_{IV,a}$ signal, surprisingly, is separated to two well-resolved cross-peaks at (50, −58) and (53, −5), as denoted in the spectrum. The clear separation of the three species in Figure 4b evidently shows that the $\delta(^{31}P)$ = −58 ppm species is uniquely different from BAS and LAS sites. A simple quadrupolar fitting of the row slice spectrum at F_1 = −58 ppm (not shown) yields C_Q of 4 MHz (corresponding to υ_Q of 0.6 MHz) for the Al species associated to the (50, −58) cross-peak, while the actual C_Q shall be smaller as chemical shift distribution may contribute to part of the linewidth. Such a small quadrupolar coupling constant ensures reliable analysis of the ^{31}P{^{27}Al} CP REAPDOR experiments discussed above. More intriguing findings can be observed in the ^{27}Al{^{1}H} *D*-RINEPT result in Figure 4c where the cross-peak at F_2 = 1.7 ppm arises from overlapped signals of methyl groups on all titrated sites, and by comparing with Figure 4b, the (6.3, 53) signal can be unambiguously assigned to the BAS-TMP site and the (7.0, 49) signal marked in yellow should be responsible for the $\delta(^{31}P)$ = −58 ppm species. However, one can easily notice that in the interested yellow-marked region, the ^{1}H chemical shift does not exactly match that in the ^{1}H-^{31}P spectra in Figure 2. This indicates a *complex environment* for the Al−OH groups where significant proton chemical shift distribution exists, i.e., a fraction of the protons closer to the P atom and others closer to Al atoms; in contrast, the more crystalline BAS-TMP site yields a consistent ^{1}H chemical shift at 6.3 ppm in all cases. In addition, ^{1}H DQ-SQ NMR (with ^{31}P *J*-decoupling) experiment, a common method to simplify the ^{1}H spectroscopy by selecting homonuclear correlations,[13,72] clearly resolves the two proton species at 6.3 and 7.8 ppm, and importantly, reveals their correlations with the methyl group on TMP at 1.8 and 1.0 ppm, respectively, as marked in blue and yellow in Figure 4d. Notably, a relatively larger chemical shift distribution is observed on the 7.8 ppm species compared to the 6.3 ppm species, indicated by its more "stretched" cross-peak lineshape,[47] again suggesting a more complex environment of such species. With all the evidence above, it can be concluded that the $\delta(^{31}P)$ = −58 ppm species corresponds to TMP adsorbed on Al−OH associated to the partially framework-coordinated Al species, i.e., "Al(IV)-2" as reported recently,[10,11,13] as demonstrated in the structural scheme in Figure 4e. It must be clarified that these schemes are only for illustration purposes; the exact binding location of TMP on Al(IV)-2 is still not clear with the current evidence and remains as a challenging problem as complex hydrogen bonding network might exist around the actual Al(IV)-2 species.

The assignment is further supported by postsynthetic treatments to the catalyst as control experiments, i.e., via steaming and ammonium hexafluorosilicate (AHFS) wash processes, which are typically used to create and remove EFAl[73−75] and Al(IV)-2 species.[10,11] As the as-received H-form ZSM-5 catalyst with Si/Al = 19 (P-ZSM-5) purchased from

https://doi.org/10.1021/acscatal.3c00714
ACS Catal. 2023, 13, 4960−4970

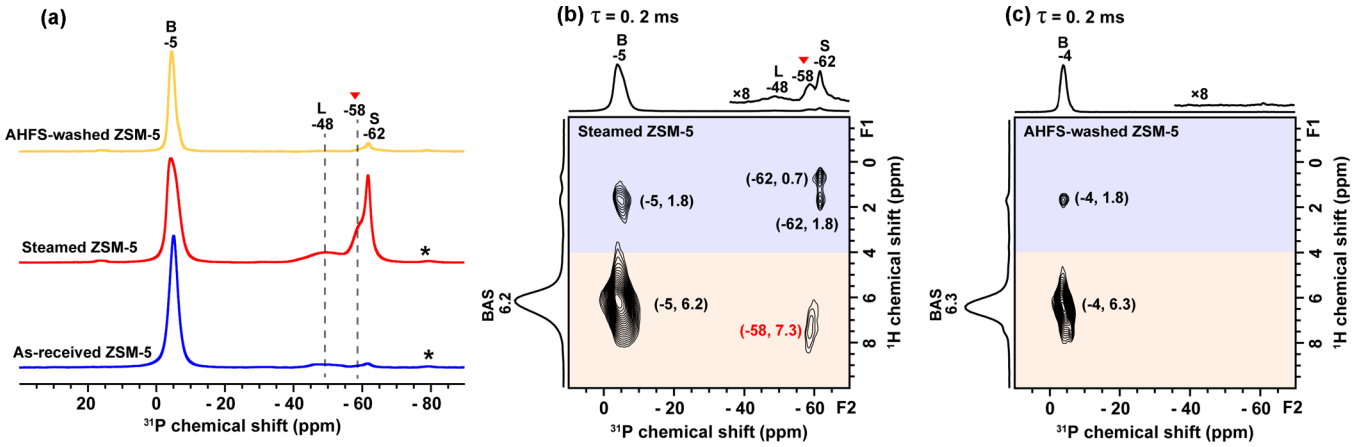

Figure 5. (a) $^{31}P\{^{1}H\}$ CP MAS NMR spectra of TMP adsorbed on dehydrated as-received, steamed, and AHFS-washed ZSM-5 catalysts with Si/Al = 11.5, showing the creation and removal of the −48 and −58 ppm peaks upon steaming and AHFS washing. (b,c) Corresponding 2D ^{1}H-^{31}P HETCOR MAS NMR spectra (with ^{31}P *J*-decoupling) of the "steamed" and "AHFS-washed" catalysts with a contact time of 0.2 ms. All spectra are acquired at 9.4 T.

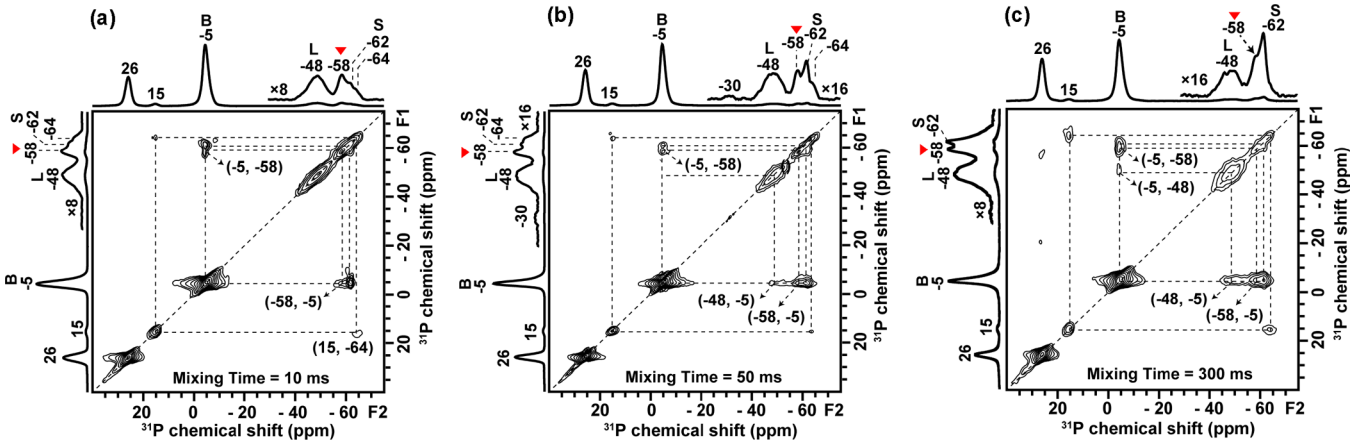

Figure 6. ^{31}P-^{31}P CORD MAS NMR spectra of C-ZSM-5 after TMP adsorption recorded with mixing times of (a) 10 ms, (b) 50 ms, and (c) 300 ms. The off-diagonal cross-peaks arise from sites that are spatially proximate. The interested −58 ppm signal is indicated by red triangles in the projections in each figure. The enlarged sections of the corresponding spectra from 9 to −74 ppm are shown in Figure S9. All spectra are acquired at 14.1 T.

Nankai initially contains appreciable amounts of EFAl and Al(IV)-2 species (see the ^{27}Al MAS spectrum in Figure S6a), the control experiment was carried out on ZSM-5 catalysts with Si/Al = 11.5 purchased from Zeolyst International, Inc., which is nearly free of EFAl and Al(IV)-2 species (see Figure S6a). The "as-received," "steamed," and "steamed then AHFS-washed" catalysts are all treated with TMP with their 1D $^{31}P\{^{1}H\}$ CP and 2D ^{1}H-^{31}P HETCOR spectra illustrated in Figure 5. Figure 5a shows that the signal at −58 ppm is remarkably enhanced upon steaming and disappears after AHFS washing, which is also clearly demonstrated in the 2D ^{1}H-^{31}P HETCOR spectra in Figure 5b,c. Furthermore, the ^{31}P-^{27}Al *D*-HMQC MAS NMR spectrum of steamed ZSM-5 (Si/Al = 11.5) in Figure S7a shows an identical pattern with that of C-ZSM-5 (Si/Al = 19) illustrated in Figure 4b. Meanwhile, only the correlation signals related to BAS remain in the ^{27}Al-^{1}H *D*-RINEPT spectrum (Figure S7b) for the AHFS-washed sample. It is important to emphasize that the −58 ppm species created by steaming is similar in almost all spectroscopical means (see Figures 5, S7, and S8) compared to that created by calcination (Figures 1 and 2) even though the fundamental dealumination process might differ with and without the presence of water molecules. It is also worth noting that as an experimental observation, the −58 ppm species is more efficiently created by the steaming method, indicated by the more enhanced −58 ppm peak in steamed ZSM-5 catalysts (Si/Al = 11.5) in the ^{31}P spectra in Figure S8a, compared to the calcined catalyst in Figure S2a, which is consistent with the fact that Al(IV)-2 is formed by water-mediated dealumination processes.[12,62,76]

Proximity among Various Acid Sites. With the identity of the $\delta(^{31}P)$ = −58 ppm species confirmed, its spatial proximity with other catalytic sites can be better revealed by ^{31}P-^{31}P homonuclear correlation NMR experiments than the often used ^{1}H-^{1}H correlation,[14,77,78] provided ^{31}P has much longer spin−lattice relaxation time and chemical exchange can be excluded, which is a practical problem for the latter due to water-mediated proton-hopping mechanisms even at catalytic amounts.[79−83] Note that the chemical exchange is excluded also due to the small pore size of ZSM-5 channels (ca. 5−6 Å) compared to the effective TMP diameter (5.5 Å).[61] Because of the wide chemical shift range of the ^{31}P spectrum, the CORD method was employed to establish the 2D ^{31}P-^{31}P homonuclear NMR correlation[43,75] as it is suitable for yielding

https://doi.org/10.1021/acscatal.3c00714
ACS Catal. 2023, 13, 4960−4970

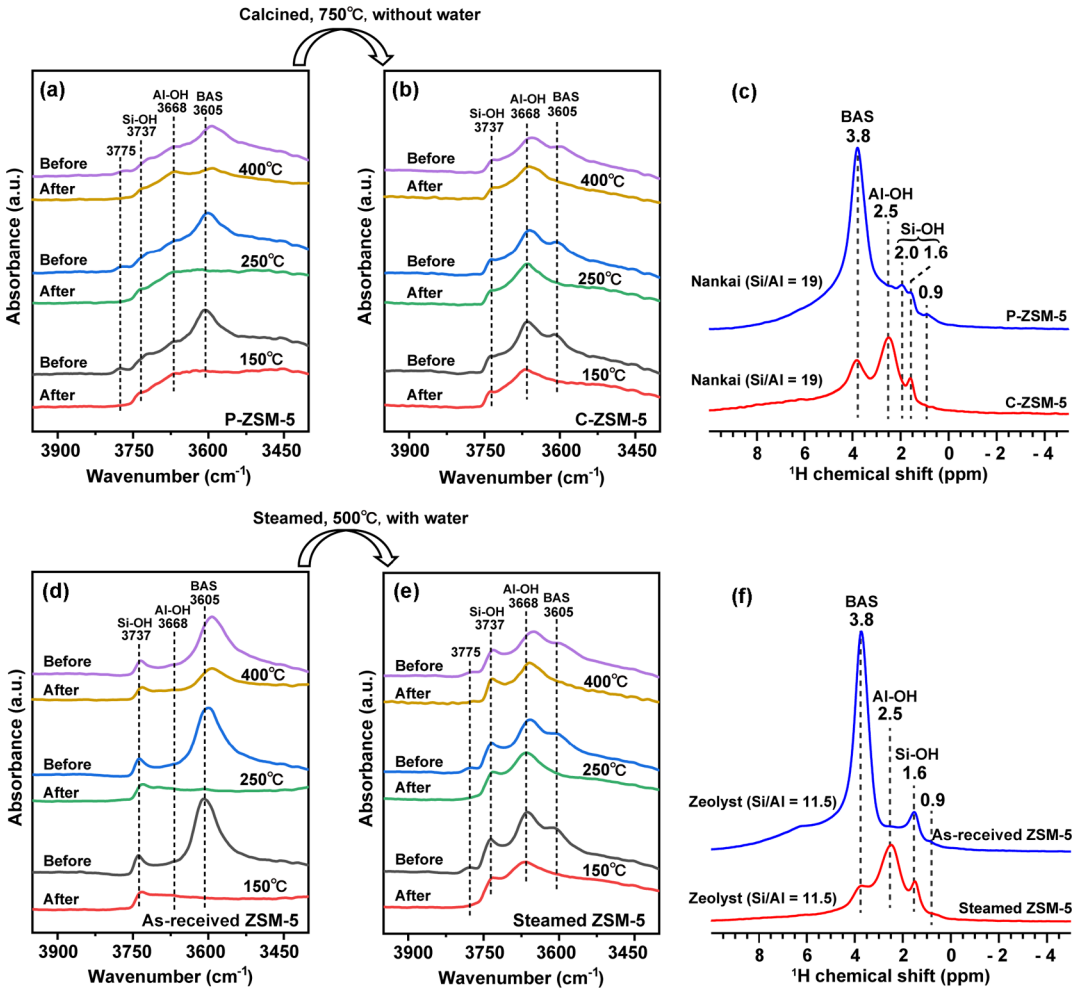

Figure 7. FTIR spectra of calcination (a,b) and steaming (d,e) thermal treatments on HZSM-5 catalysts and ^{1}H MAS NMR spectra (c,f) of each catalyst as indicated in the figure. Also, each catalyst was probed with pyridine at variable temperatures (150, 250, and 400 °C), labeled as "before" and "after" to indicate the absence and presence of pyridine treatment. Note that the steaming process is performed on ZSM-5 (Si/Al = 11.5) catalysts obtained from Zeolyst as it contains little initial EFAls and Al(IV)-2.

uniform distribution of cross-peaks due to its advantage in broadband homonuclear dipolar recoupling. Figure 6 illustrates the 2D ^{31}P-^{31}P CORD spectra with mixing times of 10, 50, and 300 ms. Benefiting from long T_1 values of ^{31}P, even at 300 ms, all correlations continue to grow and more defined patterns could be established compared to ^{1}H-^{1}H correlation experiments. The off-diagonal correlation peak at (15, −64) shows that the 15 ppm species is likely related to silanols, and thus, importantly, its identity does not affect the interpretation of the −58 ppm species. The cross-peaks at (−5, −58)/(−58, −5) and (−5, −62)/(−62, −5) were observed at the shortest mixing time of 10 ms (Figure 6a), indicating close proximity between Al(IV)-2 and BAS, in agreement with a recent finding that Al(IV)-2 is preferably created near BAS during dealumination processes.[13] By increasing the mixing time to 50 ms (Figure 6b), the (−48, −5) correlation appears, indicating BAS/LAS proximity, but possibly in longer distances than the BAS/Al(IV)-2 pair. To the best of our knowledge, such a direct comparison between the two pairs has not yet been reported. Semi-quantitative distances between these pairs were further determined using the ^{31}P-^{31}P RFDR experiment,[44−46] which are 7.0 and 5.3 Å, respectively, as illustrated in Figure S10. This result provides a great opportunity to address the recently debated BAS/LAS[14,49,51] and BAS/BAS[50] synergy arguments. Also, it is worth noting that the correlation between Al(IV)-2 and LAS has never been observed, which is plausible as both are derived from BAS during dealumination, and the formation of Al(IV)-2/LAS pairs requires simultaneous dealumination on adjacent BAS's, which is statistically unfavored.

Identity, Evolution, and Acidity of Partially Framework-Bonded Al Species upon Thermal Treatment. In contrast to NMR, FTIR was employed to investigate the calcination and steaming treatments on HZSM-5 catalysts for complementary insights of evolution of Al species. The catalysts are also probed by pyridine at variable temperatures to assist analyzing the acidity of active sites. Figure 7 illustrates the FTIR results along with the ^{1}H NMR spectra for a direct comparison. The bands near 3605 and 3737 cm^{-1} are well known to arise from BAS and silanol groups, respectively.[84−88] The bands near 3775 and 3668 cm^{-1}, although both are assigned to aluminol groups, still remain controversial between EFAls (totally dislodged from framework)[73,89] and partially framework-bonded aluminols[90−93] as of detailed structural identities, the terms of which are often mixed-used.[73,89,90,94−96] Interestingly, the IR and ^{1}H NMR spectra appear in similar patterns with respect to Si−OH, Al−OH, and BAS species (both position and intensity) but in a reversed order compared with the IR

https://doi.org/10.1021/acscatal.3c00714
ACS Catal. 2023, 13, 4960−4970

and ^{1}H NMR spectra of the same sample, e.g., "Figure 7a vs c (top)" and "Figure 7b vs c (bottom)." This trend is reasonable because normally increased bond strengths lead to IR absorbances with higher wavenumbers, and increased bond strengths are also likely associated with more electron overlaps, and hence more electron shieldings, which will result in smaller chemical shifts (in ppm unit). Such IR-^{1}H NMR correlation for zeolites has also been verified by DFT calculations in a recent study.[94] Therefore, the IR bands at 3775 and 3668 cm^{-1} could be associated to the 0.9 and 2.5 ppm species in the ^{1}H NMR spectrum. With this NMR-IR correlation, the 3668 cm^{-1} species could be associated to Al(IV)-2 but not EFAls as the 2.5 ppm ^{1}H NMR species has been verified as Al(IV)-2 in recent studies.[10,11] Figure 7b,e shows that the 3668 cm^{-1} absorbance reduces partially upon adsorption of pyridine at 150 °C and almost completely recovered by increasing the temperature to 250 and 400 °C. In comparison, BAS at 3605 cm^{-1} is still largely titrated by pyridine even at the highest temperature 400 °C. This apparently weaker acidity of Al(IV)-2 could be attributed to the steric issues due to its complex hydrogen bonding environment. However, one should note that acidity only attributes partly to the activity of the active site, while synergistic effect and/or local confinement are also other crucial, if not more important factors, and both of which can be greatly altered by the hydroxyl-rich Al(IV)-2 site. NH_3-TPD analysis was carried out to probe the total acid densities as shown in Figure S11. For both calcination and steaming processes, the total acid density all dropped by as large as 70%, indicating that severe hydroxyl condensation occurred in both cases, in accordance with the decreased total proton intensities in Figure 7c,f upon each thermal treatment. Also, the center of the "strong acid" peak is further shifted to the lower temperature range by the calcination process compared to that by the steaming process, implying a decrease of the apparent acidity. Maybe the steaming process creates more synergistic effects that can stabilize the NH_3 molecules. However, one should always carefully treat the NH_3-TPD result as it is not site-specific and only provides overall effects.

The assignment and importance of the 3775 cm^{-1} species would be worth further discussion despite its small quantity. First, this species should be the same species discussed previously with IR absorbances at >3780 cm^{-1} on various types of zeolites although it appears in a slightly lower frequency.[90−93,95] Brand et al. proposed that it arises from terminal Al−OH groups based on theoretical studies of IR shifts using a modeling molecule, dimeric $(Al(OH)_3)_2$.[95] Vimont et al. proposed the species as a hydroxyl group attached to a tri-coordinated aluminum atoms bonded to framework based on pyridine/IR probing experiments;[90] a similar proposal was also raised by Kiricsi et al. upon very deliberated IR studies on a series of probe molecules such as pyridine, benzene, and hexane.[91] What is also clear is this species exhibits acidity given its interaction with different probe molecules,[90,91] including CO molecule at 77 K.[92] Here, the pyridine adsorption data in Figure 7 show that all the 3775 cm^{-1} species can be titrated by pyridine, which further verifies that this is the same species as of the >3780 cm^{-1} species discussed in the past. Notably, an interesting phenomenon is observed: such species is removed by calcination at 750 °C (Figure 7a vs b) but produced by steaming at 500 °C (Figure 7d vs e). The disappearance of the 3775 cm^{-1} absorbance in Figure 7b strongly suggests that this species is not EFAl or at least not EFAl species typically characterized in fully hydrated zeolites near 30 ppm (penta-coordinated) and 0 ppm (octa-coordinated) in ^{27}Al NMR of the catalyst as shown in Figure S6b. It is likely hydroxyl group condensations at such a high temperature, and the absence of water caused the disappearance of the 3775 cm^{-1} absorbance. On the contrary, the fact that steaming can easily produce this species strongly implies it being partially framework-bonded species, of which the formation is favored by the presence of water.[12,62,76] It is worth mentioning that the 3775 cm^{-1} absorbance is not recovered even at 400 °C degassing pyridine, which indicates stronger bindings compared to BAS and Al(IV)-2 at 3605 and 3668 cm^{-1}. Thus, it can possibly be attributed to framework-bonded Lewis acid sites (e.g., tri-coordinated Al). In all, IR-NMR correlation and the clarification of the high-frequency IR species at 3775 cm^{-1} might provide insights to untangle the long-lasting debates about framework, nonframework, and partially framework-bonded Al species.

CONCLUSIONS

Efficient means of characterizing structurally similar active sites are urgently needed, especially for the increased recognition of complex hydroxyl groups in zeolites. In this work, with a combination of modern ssNMR techniques, including 1D ^{31}P MAS and ^{31}P{^{27}Al} CP REAPDOR, and 2D ^{1}H-^{31}P HETCOR, ^{31}P-^{27}Al *D*-HMQC, and ^{27}Al MQMAS experiments, as well as a set of postsynthetic treatments, we were able to show unambiguously that for TMP-treated zeolites, a unique ^{31}P resonance at −58 ppm, which used to be treated as inert species, exclusively arises from TMP molecules adsorbed on Al−OH groups associated to the recently reported partially framework-coordinated Al species, as denoted "Al(IV)-2" usually. IR and ^{1}H NMR spectroscopical results all together helped to clarify Al(IV)-2 (essentially Brønsted sites) and framework-bonded Lewis sites in spectroscopy. Furthermore, ^{31}P-^{31}P homonuclear correlation experiments were capable of ruling out chemical exchange from spin diffusion and thereby exclusively demonstrate that the "BAS and Al(IV)-2" is in shorter spatial distance than that of "BAS and LAS." The comprehensive demonstration of characterizing the TMP/Al(IV)-2 in this work clarifies the remaining problems in previous studies using ^{31}P NMR TMP probe technique, and the addressment of the catalytic site proximities may shed light on the structure−function relationship in catalytic reactions.

ASSOCIATED CONTENT

Supporting Information

The Supporting Information is available free of charge at https://pubs.acs.org/doi/10.1021/acscatal.3c00714.

Sample preparations, experimental details including XRD patterns, NH_3-TPD curves and of NMR experiments such as single-pulse ^{31}P MAS, ^{31}P{^{1}H} CP, ^{1}H MAS, ^{27}Al MAS, double resonance ^{31}P{^{27}Al} CP REAPDOR, and two-dimensional (2D) correlation experiments ^{31}P-^{27}Al *D*-HMQC, ^{27}Al-^{1}H *D*-RINEPT, ^{31}P-^{31}P CORD MAS NMR, and ^{31}P-^{31}P RFDR MAS NMR (PDF)

AUTHOR INFORMATION

Corresponding Authors

Kuizhi Chen − *State Key Laboratory of Catalysis, Dalian Institute of Chemical Physics, Chinese Academy of Sciences,*

https://doi.org/10.1021/acscatal.3c00714
ACS Catal. 2023, 13, 4960−4970

Dalian 116023, China; orcid.org/0000-0002-9853-7070; Email: kchen@dicp.ac.cn

Shutao Xu − *State Key Laboratory of Catalysis, Dalian Institute of Chemical Physics, Chinese Academy of Sciences, Dalian 116023, China;* orcid.org/0000-0003-4722-8371; Email: xushutao@dicp.ac.cn

Guangjin Hou − *State Key Laboratory of Catalysis, Dalian Institute of Chemical Physics, Chinese Academy of Sciences, Dalian 116023, China;* orcid.org/0000-0001-8216-863X; Email: ghou@dicp.ac.cn

Authors

Zhili Wang − *State Key Laboratory of Catalysis, Dalian Institute of Chemical Physics, Chinese Academy of Sciences, Dalian 116023, China; University of Chinese Academy of Sciences, Beijing 100049, China;* orcid.org/0000-0002-5793-0730

Dong Xiao − *State Key Laboratory of Catalysis, Dalian Institute of Chemical Physics, Chinese Academy of Sciences, Dalian 116023, China*

Caiyi Lou − *State Key Laboratory of Catalysis, Dalian Institute of Chemical Physics, Chinese Academy of Sciences, Dalian 116023, China; University of Chinese Academy of Sciences, Beijing 100049, China*

Lixin Liang − *State Key Laboratory of Catalysis, Dalian Institute of Chemical Physics, Chinese Academy of Sciences, Dalian 116023, China; University of Chinese Academy of Sciences, Beijing 100049, China*

Complete contact information is available at: https://pubs.acs.org/10.1021/acscatal.3c00714

Author Contributions

All authors have given approval to the final version of the manuscript.

Notes

The authors declare no competing financial interest.

■ ACKNOWLEDGMENTS

We are grateful for the financial supports from the National Key Research and Development Program of China (Nos. 2022YFA1504500 and 2022YFA1504800), the National Natural Science Foundation of China (Nos. 21773230, 91945302, 21972142, 22022202, and 22002165), LiaoNing Revitalization Talents Program (XLYC1807207), and DICP & QIBEBT UN201808. We are also grateful for Yuting Sun for preparing the AHFS-washed catalysts and Yilun Ding for conducting the NH_3-TPD experiments.

■ REFERENCES

(1) Weitkamp, J. Zeolites and Catalysis. *Solid State Ionics* **2000**, *131*, 175−188.

(2) Weckhuysen, B. M.; Yu, J. Recent Advances in Zeolite Chemistry and Catalysis. *Chem. Soc. Rev.* **2015**, *44*, 7022−7024.

(3) Hunger, M. Multinuclear Solid-State NMR Studies of Acidic and Non-Acidic Hydroxyl Protons in Zeolites. *Solid State Nucl. Magn. Reson.* **1996**, *6*, 1−29.

(4) Eder, F.; Stockenhuber, M.; Lercher, J. A. Brønsted Acid Site and Pore Controlled Siting of Alkane Sorption in Acidic Molecular Sieves. *J. Phys. Chem. B* **1997**, *101*, 5414−5419.

(5) Hunger, M. Brønsted Acid Sites in Zeolites Characterized by Multinuclear Solid-State NMR Spectroscopy. *Catal. Rev.: Sci. Eng.* **1997**, *39*, 345−393.

(6) Maier, S. M.; Jentys, A.; Lercher, J. A. Steaming of Zeolite Bea and Its Effect on Acidity: A Comparative NMR and IR Spectroscopic Study. *J. Phys. Chem. C* **2011**, *115*, 8005−8013.

(7) Ravi, M.; Sushkevich, V. L.; Van Bokhoven, J. A. Towards a Better Understanding of Lewis Acidic Aluminium in Zeolites. *Nat. Mater.* **2020**, *19*, 1047−1056.

(8) Hu, M.; Wang, C.; Chu, Y.; Wang, Q.; Li, S.; Xu, J.; Deng, F. Unravelling the Reactivity of Framework Lewis Acid Sites Towards Methanol Activation on H-ZSM-5 Zeolite with Solid-State NMR Spectroscopy. *Angew. Chem., Int. Ed.* **2022**, *61*, No. e202207400.

(9) Corma, A.; García, H. Lewis Acids: From Conventional Homogeneous to Green Homogeneous and Heterogeneous Catalysis. *Chem. Rev.* **2003**, *103*, 4307−4366.

(10) Chen, K.; Horstmeier, S.; Nguyen, V. T.; Wang, B.; Crossley, S. P.; Pham, T.; Gan, Z.; Hung, I.; White, J. L. Structure and Catalytic Characterization of a Second Framework Al(IV) Site in Zeolite Catalysts Revealed by NMR at 35.2 T. *J. Am. Chem. Soc.* **2020**, *142*, 7514−7523.

(11) Chen, K.; Gan, Z.; Horstmeier, S.; White, J. L. Distribution of Aluminum Species in Zeolite Catalysts: ^{27}Al NMR of Framework, Partially-Coordinated Framework, and Non-Framework Moieties. *J. Am. Chem. Soc.* **2021**, *143*, 6669−6680.

(12) Silaghi, M.-C.; Chizallet, C.; Sauer, J.; Raybaud, P. Dealumination Mechanisms of Zeolites and Extra-Framework Aluminum Confinement. *J. Catal.* **2016**, *339*, 242−255.

(13) Chen, K.; Zornes, A.; Nguyen, V.; Wang, B.; Gan, Z.; Crossley, S. P.; White, J. L. ^{17}O Labeling Reveals Paired Active Sites in Zeolite Catalysts. *J. Am. Chem. Soc.* **2022**, *144*, 16916−16929.

(14) Li, S.; Zheng, A.; Su, Y.; Zhang, H.; Chen, L.; Yang, J.; Ye, C.; Deng, F. Brønsted/Lewis Acid Synergy in Dealuminated HY Zeolite: A Combined Solid-State NMR and Theoretical Calculation Study. *J. Am. Chem. Soc.* **2007**, *129*, 11161−11171.

(15) Zhao, S.; Yang, W.; Kim, K. D.; Wang, L.; Wang, Z.; Ryoo, R.; Huang, J. Synergy of Extraframework Al^{3+} Cations and Brønsted Acid Sites on Hierarchical ZSM-5 Zeolites for Butanol-to-Olefin Conversion. *J. Phys. Chem. C* **2021**, *125*, 11665−11676.

(16) Xu, J.; Wang, Q.; Deng, F. Metal Active Sites and Their Catalytic Functions in Zeolites: Insights from Solid-State NMR Spectroscopy. *Acc. Chem. Res.* **2019**, *52*, 2179−2189.

(17) Li, S.; Zhou, L.; Zheng, A.; Deng, F. Recent Advances in Solid State NMR Characterization of Zeolites. *Chin. J. Catal.* **2015**, *36*, 789−796.

(18) Brouwer, D. H.; Darton, R. J.; Morris, R. E.; Levitt, M. H. A Solid-State NMR Method for Solution of Zeolite Crystal Structures. *J. Am. Chem. Soc.* **2005**, *127*, 10365−10370.

(19) Zheng, A.; Huang, S.-J.; Wang, Q.; Zhang, H.; Deng, F.; Liu, S.-B. Progress in Development and Application of Solid-State NMR for Solid Acid Catalysis. *Chin. J. Catal.* **2013**, *34*, 436−491.

(20) Schroeder, C.; Zones, S. I.; Mück-Lichtenfeld, C.; Hansen, M. R.; Koller, H. High Aluminum Ordering in SSZ-59: Residual ^{1}H−^{27}Al Dipolar Coupling Effects in ^{1}H MAS NMR Spectra of Brønsted Acid Sites in Zeolites. *J. Phys. Chem. C* **2021**, *125*, 4869−4877.

(21) Yi, X.; Ko, H. H.; Deng, F.; Liu, S. B.; Zheng, A. Solid-State ^{31}P NMR Mapping of Active Centers and Relevant Spatial Correlations in Solid Acid Catalysts. *Nat. Protoc.* **2020**, *15*, 3527−3555.

(22) Zheng, A.; Liu, S.-B.; Deng, F. Acidity Characterization of Heterogeneous Catalysts by Solid-State NMR Spectroscopy Using Probe Molecules. *Solid State Nucl. Magn. Reson.* **2013**, *55-56*, 12−27.

(23) Rothwell, W. P.; Shen, W. X.; Lunsford, J. H. ^{31}P Solid-State NMR of a Chemisorbed Phosphonium Ion in H-Y Zeolite: Observation of ^{1}H-^{31}P *J* Coupling in the Solid State. *J. Am. Chem. Soc.* **1984**, *106*, 2452−2453.

(24) Yang, W.; Wang, Z.; Huang, J.; Jiang, Y. Qualitative and Quantitative Analysis of Acid Properties for Solid Acids by Solid-State Nuclear Magnetic Resonance Spectroscopy. *J. Phys. Chem. C* **2021**, *125*, 10179−10197.

(25) Yi, X.; Liu, K.; Chen, W.; Li, J.; Xu, S.; Li, C.; Xiao, Y.; Liu, H.; Guo, X.; Liu, S.-B.; Zheng, A. Origin and Structural Characteristics of

Tri-Coordinated Extra-Framework Aluminum Species in Dealuminated Zeolites. *J. Am. Chem. Soc.* **2018**, *140*, 10764−10774.
(26) Zheng, A.; Huang, S. J.; Liu, S. B.; Deng, F. Acid Properties of Solid Acid Catalysts Characterized by Solid-State ^{31}P NMR of Adsorbed Phosphorous Probe Molecules. *Phys. Chem. Chem. Phys.* **2011**, *13*, 14889−14901.
(27) Zheng, A.; Liu, S. B.; Deng, F. ^{31}P NMR Chemical Shifts of Phosphorus Probes as Reliable and Practical Acidity Scales for Solid and Liquid Catalysts. *Chem. Rev.* **2017**, *117*, 12475−12531.
(28) Bornes, C.; Stosic, D.; Geraldes, C. F. G. C.; Mintova, S.; Rocha, J.; Mafra, L. Elucidating the Nature of the External Acid Sites of ZSM-5 Zeolites Using NMR Probe Molecules. *Chem. − Eur. J.* **2022**, No. e202201795.
(29) Gabrienko, A. A.; Danilova, I. G.; Arzumanov, S. S.; Freude, D.; Stepanov, A. G. Does the Zn^{2+} Species Introduced into H-ZSM-5 Zeolite Affect the Strength of Brønsted Acid Sites? *ChemCatChem* **2020**, *12*, 478−487.
(30) Chu, Y.; Yu, Z.; Zheng, A.; Fang, H.; Zhang, H.; Huang, S.-J.; Liu, S.-B.; Deng, F. Acidic Strengths of Brønsted and Lewis Acid Sites in Solid Acids Scaled by ^{31}P NMR Chemical Shifts of Adsorbed Trimethylphosphine. *J. Phys. Chem. C* **2011**, *115*, 7660−7667.
(31) Kao, H.-M.; Grey, C. P. Characterization of the Lewis Acid Sites in Zeolite HY with the Probe Molecule Trimethylphosphine, and ^{31}P/^{27}Al Double Resonance NMR. *Chem. Phys. Lett.* **1996**, *259*, 459−464.
(32) Lunsford, J. H.; Rothwell, W. P.; Shen, W. Acid Sites in Zeolite Y: A Solid-State NMR and Infrared Study Using Trimethylphosphine as a Probe Molecule. *J. Am. Chem. Soc.* **1985**, *107*, 1540−1547.
(33) Lunsford, J. H.; Tutunjian, P. N.; Chu, P. J.; Yeh, E. B.; Zalewski, D. Solid-State NMR Study Using Trimethylphosphine as a Probe of Acid Sites in Normal and Dealuminated Zeolite Y. *J. Phys. Chem.* **1989**, *93*, 2590−2595.
(34) Goldbourt, A.; Vega, S.; Gullion, T.; Vega, A. J. Interatomic Distance Measurement in Solid-State NMR between a Spin-1/2 and a Spin-5/2 Using a Universal REAPDOR Curve. *J. Am. Chem. Soc.* **2003**, *125*, 11194−11195.
(35) Gullion, T. Measurement of Dipolar Interactions between Spin-1/2 and Quadrupolar Nuclei by Rotational-Echo, Adiabatic-Passage Double-Resonance NMR. *Chem. Phys. Lett.* **1995**, *246*, 325−330.
(36) Santos, R. A.; Wind, R. A.; Bronnimann, C. E. ^{1}H CRAMPS and ^{1}H-^{31}P HetCor Experiments on Bone, Bone Mineral, and Model Calcium Phosphate Phases. *J. Magn. Reson. B* **1994**, *105*, 183−187.
(37) Holland, G. P.; Alam, T. M. Unique Backbone-Water Interaction Detected in Sphingomyelin Bilayers with ^{1}H/^{31}P and ^{1}H/^{13}C HETCOR MAS NMR Spectroscopy. *Biophys. J.* **2008**, *95*, 1189−1198.
(38) Dey, K. K.; Prasad, S.; Ash, J. T.; Deschamps, M.; Grandinetti, P. J. Spectral Editing in Solid-State MAS NMR of Quadrupolar Nuclei Using Selective Satellite Inversion. *J. Magn. Reson.* **2007**, *185*, 326−330.
(39) Chen, K.; Zornes, A.; Bababrik, R.; Crouch, J.; Alvarez, W.; Wulfers, M.; Resasco, D.; Wang, B.; Crossley, S.; White, J. L. First-Formed Framework Species and Phosphate Structure Distributions in Phosphorus-Modified MFI Zeolites. *J. Phys. Chem. C* **2022**, *126*, 227−238.
(40) Gómez, J. S.; Rankin, A. G.; Trébosc, J.; Pourpoint, F.; Tsutsumi, Y.; Nagashima, H.; Lafon, O.; Amoureux, J.-P. Improved NMR Transfer of Magnetization from Protons to Half-Integer Spin Quadrupolar Nuclei at Moderate and High MAS Frequencies. *Magn. Reson.* **2021**, *2*, 447−464.
(41) Venkatesh, A.; Hanrahan, M. P.; Rossini, A. J. Proton Detection of MAS Solid-State NMR Spectra of Half-Integer Quadrupolar Nuclei. *Solid State Nucl. Magn. Reson.* **2017**, *84*, 171−181.
(42) Liang, L.; Ji, Y.; Zhao, Z.; Quinn, C. M.; Han, X.; Bao, X.; Polenova, T.; Hou, G. Accurate Heteronuclear Distance Measurements at All Magic-Angle Spinning Frequencies in Solid-State NMR Spectroscopy. *Chem. Sci.* **2021**, *12*, 11554−11564.
(43) Hou, G.; Yan, S.; Trébosc, J.; Amoureux, J.-P.; Polenova, T. Broadband Homonuclear Correlation Spectroscopy Driven by Combined R2$^{v}_{n}$ Sequences under Fast Magic Angle Spinning for NMR Structural Analysis of Organic and Biological Solids. *J. Magn. Reson.* **2013**, *232*, 18−30.
(44) Ramamoorthy, A.; Xu, J. 2D ^{1}H/^{1}H RFDR and NOESY NMR Experiments on a Membrane-Bound Antimicrobial Peptide under Magic Angle Spinning. *J. Phys. Chem. B* **2013**, *117*, 6693−6700.
(45) Roos, M.; Mandala, V. S.; Hong, M. Determination of Long-Range Distances by Fast Magic-Angle-Spinning Radiofrequency-Driven ^{19}F−^{19}F Dipolar Recoupling NMR. *J. Phys. Chem. B* **2018**, *122*, 9302−9313.
(46) Pandey, M. K.; Vivekanandan, S.; Yamamoto, K.; Im, S.; Waskell, L.; Ramamoorthy, A. Proton-Detected 2D Radio Frequency Driven Recoupling Solid-State NMR Studies on Micelle-Associated Cytochrome-b$_5$. *J. Magn. Reson.* **2014**, *242*, 169−179.
(47) Chen, K. A Practical Review of NMR Lineshapes for Spin-1/2 and Quadrupolar Nuclei in Disordered Materials. *Int. J. Mol. Sci.* **2020**, *21*, 5666.
(48) Amoureux, J.-P.; Fernandez, C.; Steuernagel, S. Z Filtering in MQMAS NMR. *J. Magn. Reson.* **1996**, *123*, 116−118.
(49) Yu, Z.; Li, S.; Wang, Q.; Zheng, A.; Jun, X.; Chen, L.; Deng, F. Brønsted/Lewis Acid Synergy in H−ZSM-5 and H−MOR Zeolites Studied by ^{1}H and ^{27}Al DQ-MAS Solid-State NMR Spectroscopy. *J. Phys. Chem. C* **2011**, *115*, 22320−22327.
(50) Chen, K.; Abdolrahmani, M.; Horstmeier, S.; Pham, T. N.; Nguyen, V. T.; Zeets, M.; Wang, B.; Crossley, S.; White, J. L. Brønsted−Brønsted Synergies between Framework and Noncrystalline Protons in Zeolite H-ZSM-5. *ACS Catal.* **2019**, *9*, 6124−6136.
(51) Zheng, A.; Li, S.; Liu, S.-B.; Deng, F. Acidic Properties and Structure−Activity Correlations of Solid Acid Catalysts Revealed by Solid-State NMR Spectroscopy. *Acc. Chem. Res.* **2016**, *49*, 655−663.
(52) Mota, C. J.; Bhering, D. L.; Rosenbach, N. J., Jr. A DFT Study of the Acidity of Ultrastable Y Zeolite: Where Is the Brønsted/Lewis Acid Synergism? *Angew. Chem., Int. Ed.* **2004**, *116*, 3112−3115.
(53) Bhering, D. L.; Ramírez-Solís, A.; Mota, C. J. A. A Density Functional Theory Based Approach to Extraframework Aluminum Species in Zeolites. *J. Phys. Chem. B* **2003**, *107*, 4342−4347.
(54) Haw, J. F.; Zhang, J.; Shimizu, K.; Venkatraman, T. N.; Luigi, D.-P.; Song, W.; Barich, D. H.; Nicholas, J. B. NMR and Theoretical Study of Acidity Probes on Sulfated Zirconia Catalysts. *J. Am. Chem. Soc.* **2000**, *122*, 12561−12570.
(55) Zhao, Q.; Chen, W.-H.; Huang, S.-J.; Liu, S.-B. Qualitative and Quantitative Determination of Acid Sites on Solid Acid Catalysts. *Stud. Surf. Sci. Catal.* **2003**, *145*, 205−209.
(56) Gabrienko, A. A.; Kolganov, A. A.; Arzumanov, S. S.; Yashnik, S. A.; Kriventsov, V. V.; Freude, D.; Stepanov, A. G. Effect of Copper State in Cu/H-ZSM-5 on Methane Activation by Brønsted Acid Sites, Studied by ^{1}H MAS NMR in Situ Monitoring the H/D Hydrogen Exchange of the Alkane with Brønsted Acid Sites. *J. Phys. Chem. C* **2021**, *125*, 2182−2193.
(57) Zhao, B.; Pan, H.; Lunsford, J. H. Characterization of $[(CH_3)_3P{-}H]^+$ Complexes in Normal H-Y, Dealuminated H-Y, and H-ZSM-5 Zeolites Using ^{31}P Solid-State NMR Spectroscopy. *Langmuir* **1999**, *15*, 2761−2765.
(58) Rivera-Barrera, D.; Poveda-Jaramillo, J. C. Thermal Desorption of Trimethylphosphine (TMP) on the HY Zeolite Followed by FT-IR and ^{31}P MAS NMR. *J. Solid State Chem.* **2021**, *294*, No. 121862.
(59) Bondon, A.; Simonneaux, G. ^{31}P-NMR Investigation of Trimethylphosphine Binding to [αFe(II),βMn(II)] Hybrid Hemoglobin: A Model for Partially Liganded Species. *Biophys. Chem.* **1990**, *37*, 407−411.
(60) Bondon, A.; Petrinko, P.; Sodano, P.; Simonneaux, G. ^{31}P Chemical Shifts as Structural Probes for Heme Environments. ^{31}P-NMR Study of the Binding of Trimethyl Phosphine to Various Hemoglobins and Myoglobins. *Biochim. Biophys. Acta, Protein Struct. Mol. Enzymol.* **1986**, *872*, 163−166.
(61) Lunsford, J. H. Characterization of Acidity in Zeolites and Related Oxides Using Trimethylphosphine as a Probe. *Top. Catal.* **1997**, *4*, 91−98.

https://doi.org/10.1021/acscatal.3c00714
ACS Catal. 2023, 13, 4960−4970

(62) Liu, P.; Liu, Q.; Mei, D. Dealumination of the H-BEA Zeolite via the S_{N2} Mechanism: A Theoretical Investigation. *J. Phys. Chem. C* **2021**, *125*, 24613−24621.
(63) Jones, A. J.; Carr, R. T.; Zones, S. I.; Iglesia, E. Acid Strength and Solvation in Catalysis by MFI Zeolites and Effects of the Identity, Concentration and Location of Framework Heteroatoms. *J. Catal.* **2014**, *312*, 58−68.
(64) Kao, H.-M.; Liu, H.; Jiang, J.-C.; Lin, S.-H.; Grey, C. P. Determining the Structure of Trimethylphosphine Bound to the Brønsted Acid Site in Zeolite HY: Double-Resonance NMR and Ab Initio Studies. *J. Phys. Chem. B* **2000**, *104*, 4923−4933.
(65) Frydman, L.; Harwood, J. S. Isotropic Spectra of Half-Integer Quadrupolar Spins from Bidimensional Magic-Angle Spinning NMR. *J. Am. Chem. Soc.* **1995**, *117*, 5367−5368.
(66) Ashbrook, S. E. Recent Advances in Solid-State NMR Spectroscopy of Quadrupolar Nuclei. *Phys. Chem. Chem. Phys.* **2009**, *11*, 6892−6905.
(67) Van Bokhoven, J. A.; Koningsberger, D. C.; Kunkeler, P.; Van Bekkum, H.; Kentgens, A. P. M. Stepwise Dealumination of Zeolite Beta at Specific T-Sites Observed with ^{27}Al MAS and ^{27}Al MQ MAS NMR. *J. Am. Chem. Soc.* **2000**, *122*, 12842−12847.
(68) Medek, A.; Harwood, J. S.; Frydman, L. Multiple-Quantum Magic-Angle Spinning NMR: A New Method for the Study of Quadrupolar Nuclei in Solids. *J. Am. Chem. Soc.* **1995**, *117*, 12779−12787.
(69) Zhuang, J.; Ma, D.; Yang, G.; Yan, Z.; Liu, X.; Liu, X.; Han, X.; Bao, X.; Xie, P.; Liu, Z. Solid-State MAS NMR Studies on the Hydrothermal Stability of the Zeolite Catalysts for Residual Oil Selective Catalytic Cracking. *J. Catal.* **2004**, *228*, 234−242.
(70) Menezes, S. M. C.; Camorim, V. L.; Lam, Y. L.; San Gil, R. a. S.; Bailly, A.; Amoureux, J. P. Characterization of Extra-Framework Species of Steamed and Acid Washed Faujasite by MQMAS NMR and IR Measurements. *Appl. Catal., A* **2001**, *207*, 367−377.
(71) Wang, Z.; Chu, W.; Zhao, Z.; Liu, Z.; Chen, H.; Xiao, D.; Gong, K.; Li, F.; Li, X.; Hou, G. The Role of Organic and Inorganic Structure-Directing Agents in Selective Al Substitution of Zeolite. *J. Phys. Chem. Lett.* **2021**, *12*, 9398−9406.
(72) Hohwy, M.; Jakobsen, H. J.; Edén, M.; Levitt, M. H.; Nielsen, N. C. Broadband Dipolar Recoupling in the Nuclear Magnetic Resonance of Rotating Solids: A Compensated C7 Pulse Sequence. *J. Chem. Phys.* **1998**, *108*, 2686−2694.
(73) Schallmoser, S.; Ikuno, T.; Wagenhofer, M. F.; Kolvenbach, R.; Haller, G. L.; Sanchez-Sanchez, M.; Lercher, J. A. Impact of the Local Environment of Brønsted Acid Sites in ZSM-5 on the Catalytic Activity in n-Pentane Cracking. *J. Catal.* **2014**, *316*, 93−102.
(74) Abdolrahmani, M.; Chen, K.; White, J. L. Assessment, Control, and Impact of Brønsted Acid Site Heterogeneity in Zeolite HZSM-5. *J. Phys. Chem. C* **2018**, *122*, 15520−15528.
(75) Chen, K.; Abdolrhamani, M.; Sheets, E.; Freeman, J.; Ward, G.; White, J. L. Direct Detection of Multiple Acidic Proton Sites in Zeolite HZSM-5. *J. Am. Chem. Soc.* **2017**, *139*, 18698−18704.
(76) Stanciakova, K.; Ensing, B.; Göltl, F.; Bulo, R. E.; Weckhuysen, B. M. Cooperative Role of Water Molecules During the Initial Stage of Water-Induced Zeolite Dealumination. *ACS Catal.* **2019**, *9*, 5119−5135.
(77) Gao, W.; Qi, G.; Wang, Q.; Wang, W.; Li, S.; Hung, I.; Gan, Z.; Xu, J.; Deng, F. Dual Active Sites on Molybdenum/ZSM-5 Catalyst for Methane Dehydroaromatization: Insights from Solid-State NMR Spectroscopy. *Angew. Chem., Int. Ed.* **2021**, *60*, 10709−10715.
(78) Gao, P.; Wang, Q.; Xu, J.; Qi, G.; Wang, C.; Zhou, X.; Zhao, X.; Feng, N.; Liu, X.; Deng, F. Brønsted/Lewis Acid Synergy in Methanol-to-Aromatics Conversion on Ga-Modified ZSM-5 Zeolites, As Studied by Solid-State NMR Spectroscopy. *ACS Catal.* **2017**, *8*, 69−74.
(79) White, J. L.; Beck, L. W.; Haw, J. F. Characterization of Hydrogen Bonding in Zeolites by Proton Solid-State NMR Spectroscopy. *J. Am. Chem. Soc.* **1992**, *114*, 6182−6189.
(80) Kanellopoulos, J.; Gottert, C.; Schneider, D.; Knorr, B.; Prager, D.; Ernst, H.; Freude, D. NMR Investigation of Proton Mobility in Zeolites. *J. Catal.* **2008**, *255*, 68−78.
(81) Ryder, J. A.; Chakraborty, A. K.; Bell, A. T. Density Functional Theory Study of Proton Mobility in Zeolites: Proton Migration and Hydrogen Exchange in ZSM-5. *J. Phys. Chem. B* **2000**, *104*, 6998−7011.
(82) Alberti, A.; Martucci, A. Proton Transfer Mediated by Water: Experimental Evidence by Neutron Diffraction. *J. Phys. Chem. C* **2010**, *114*, 7767−7773.
(83) Losch, P.; Joshi, H. R.; Vozniuk, O.; Grünert, A.; Ochoa-Hernández, C.; Jabraoui, H.; Badawi, M.; Schmidt, W. Proton Mobility, Intrinsic Acid Strength, and Acid Site Location in Zeolites Revealed by Varying Temperature Infrared Spectroscopy and Density Functional Theory Studies. *J. Am. Chem. Soc.* **2018**, *140*, 17790−17799.
(84) Cao, K.; Fan, D.; Li, L.; Fan, B.; Wang, L.; Zhu, D.; Wang, Q.; Tian, P.; Liu, Z. Insights into the Pyridine-Modified MOR Zeolite Catalysts for DME Carbonylation. *ACS Catal.* **2020**, *10*, 3372−3380.
(85) Trombetta, M.; Armaroli, T.; Gutièrrez Alejandre, A. D.; Ramirez Solis, J.; Busca, G. An FT-IR Study of the Internal and External Surfaces of HZSM5 Zeolite. *Appl. Catal., A* **2000**, *192*, 125−136.
(86) Trombetta, M.; Busca, G.; Rossini, S.; Piccoli, V.; Cornaro, U. FT-IR Studies on Light Olefin Skeletal Isomerization Catalysis: II. The Interaction of C4 Olefins and Alcohols with HZSM5 Zeolite. *J. Catal.* **1997**, *168*, 349−363.
(87) Zhang, W.; Smirniotis, P. G.; Gangoda, M.; Bose, R. N. Brønsted and Lewis Acid Sites in Dealuminated ZSM-12 and β Zeolites Characterized by NH_3-STPD, FT-IR, and MAS NMR Spectroscopy. *J. Phys. Chem. B* **2000**, *104*, 4122−4129.
(88) Topsøe, N.-Y.; Pedersen, K.; Derouane, E. G. Infrared and Temperature-Programmed Desorption Study of the Acidic Properties of ZSM-5-Type Zeolites. *J. Catal.* **1981**, *70*, 41−52.
(89) Jiao, J.; Altwasser, S.; Wang, W.; Weitkamp, J.; Hunger, M. State of Aluminum in Dealuminated, Nonhydrated Zeolites Y Investigated by Multinuclear Solid-State NMR Spectroscopy. *J. Phys. Chem. B* **2004**, *108*, 14305−14310.
(90) Vimont, A.; Thibault-Starzyk, F.; Lavalley, J. C. Infrared Spectroscopic Study of the Acidobasic Properties of Beta Zeolite. *J. Phys. Chem. B* **2000**, *104*, 286−291.
(91) Kiricsi, I.; Flego, C.; Pazzuconi, G.; Parker, W. J.; Millini, R.; Perego, C.; Bellussi, G. Progress toward Understanding Zeolite. Beta. Acidity: An IR and ^{27}Al NMR Spectroscopic Study. *J. Phys. Chem.* **1994**, *98*, 4627−4634.
(92) Zecchina, A.; Bordiga, S.; Spoto, G.; Scarano, D.; Petrini, G.; Leofanti, G.; Padovan, M.; Arean, C. O. Low-Temperature Fourier-Transform Infrared Investigation of the Interaction of Co with Nanosized ZSM5 and Silicalite. *J. Chem. Soc., Faraday Trans.* **1992**, *88*, 2959−2969.
(93) Omegna, A.; Vasic, M.; Anton Van Bokhoven, J.; Pirngruber, G.; Prins, R. Dealumination and Realumination of Microcrystalline Zeolite Beta: An XRD, FTIR and Quantitative Multinuclear (MQ) MAS NMR Study. *Phys. Chem. Chem. Phys.* **2004**, *6*, 447−452.
(94) Treps, L.; Demaret, C.; Wisser, D.; Harbuzaru, B.; Méthivier, A.; Guillon, E.; Benedis, D. V.; Gomez, A.; Bruin, T. D.; Rivallan, M.; Catita, L.; Lesage, A.; Chizallet, C. Spectroscopic Expression of the External Surface Sites of H-ZSM-5. *J. Phys. Chem. C* **2021**, *125*, 2163−2181.
(95) Brand, H. V.; Redondo, A.; Hay, P. J. Theoretical Studies of Co Adsorption on H-ZSM-5 and Hydrothermally Treated H-ZSM-5. *J. Mol. Catal. A: Chem.* **1997**, *121*, 45−62.
(96) Holzinger, J.; Beato, P.; Lundegaard, L. F.; Skibsted, J. Distribution of Aluminum over the Tetrahedral Sites in ZSM-5 Zeolites and Their Evolution after Steam Treatment. *J. Phys. Chem. C* **2018**, *122*, 15595−15613.

https://doi.org/10.1021/acscatal.3c00714
ACS Catal. 2023, 13, 4960−4970